

Fusion and Merging of Multispectral Images using Multiscale Fundamental Forms

Paul Scheunders, Steve De Backer

Vision Lab, Department of Physics, University of Antwerp,

Groenenborgerlaan 171, 2020 Antwerpen, Belgium

Tel.: +32/3/218 04 39

Fax: +32/3/218 03 18

Email: {scheun},{debacker}@ruca.ua.ac.be

Abstract

In this paper, a new multispectral image wavelet representation is introduced, based on multiscale fundamental forms. This representation describes gradient information of multispectral images in a multiresolution framework. The representation is in particular extremely suited for the fusion and merging of multispectral images. For fusion as well as for merging, a strategy is described. Experiments are performed on multispectral images, where Landsat Thematic Mapper images are fused and merged with SPOT Panchromatic images. The proposed techniques are compared to wavelet-based techniques described in the literature.

OCIS Codes: Digital Image Processing, Image Analysis, Image Enhancement, Wavelets, Multispectral Image Fusion and Merging.

I. INTRODUCTION

Many image processing and analysis techniques make use of the image edge information, that is contained in the image gradient. This paper deals with vector-valued images, examples of which are vector-valued images are color images, medical images obtained using different imaging modalities (MRI, CT, ...) and remote sensing multispectral images. When dealing with vector-valued images, the concept of gradient needs to be reconsidered. A nice way of describing edges of vector-valued images is given in [1]. Here, the images "first fundamental form", a quadratic form, is defined for each image point. This is a local measure of directional contrast based upon the gradients of the image components. This measure is maximal in a particular direction, that in the greylevel case is the direction of the gradient. Based on this definition, in [2], a colour edge detection algorithm was described and a colour image anisotropic diffusion algorithm was described in [3].

In this paper, a new vector-valued image wavelet representation is presented. This representation allows for a multiscale edge description of vector-valued images. The idea for the representation is based on the first fundamental form of [1] and the dyadic wavelet representation of Mallat, presented in [4]. The latter decomposes an image into detail images that are convolutions of the image with derivatives of a smoothing function. These detail images can be written as the derivatives of the image, smoothed at different scales. This observation allows for a definition of multiscale fundamental forms. The eigenvectors and eigenvalues of these quadratic forms describe the directions and rates of change of the vector-valued image at that particular scale.

In this paper we will apply this concept to the problem of fusion and merging of multispectral images. A recent overview of the problem of multispectral image fusion and merging is given in [5]. We define image fusion as the combination of several bands of a vector-valued image into one greylevel image. Applications are image enhancement for visualization and reduction of the complexity of classification tasks [6], [7], [8], [9]. We will refer to image merging as the process of combining a greylevel image with each band of a vector-valued image in order to improve the spatial resolution of the vector-valued image. Applications are the combination of a high-resolution greylevel image with a low-resolution multispectral image to obtain high-resolution multispectral information [10], [11], [12]. An

example is given by the merging of SPOT Panchromatic data with Landsat Thematic Mapper multispectral images [13], [14], [15], [16], [17].

Most of the fusion and merging techniques described in the literature are pixel-based. Many techniques are based on multiresolution processing. The multiresolution approach allows for a combination of edge information at different scales. A very popular paradigm is given by the wavelet transform [10], [6], [15], [9]. Other methods, like pyramid-based fusion were also described [18], [19]. The rule for combining the detail information is an important issue. The most common rule for fusion is to take the detail coefficient from one of the bands (e.g. the one with highest energy). For merging the most common rule is substitution (e.g. substitution of the detail images of a high-resolution greylevel image into the wavelet representation of a lower-resolution multispectral image). In a concept, called ARSIS, the statistics of the detail coefficients are modelled before substitution [17]. In both cases, using the simple combination rules, important information can be lost. In the case of fusion, other bands than the one containing the maximum can contribute to an improved visualization. In the case of merging, the low-resolution band that is substituted by the high resolution image can contain important directional information, that is not present in the substituted image.

Instead, we propose to use other rules, based on the concept of Multiscale Fundamental Forms. This concept allows for a detailed simultaneous description of directional information of all bands involved. We will demonstrate that this description is extremely useful for designing fusion and merging strategies.

The paper is organized as follows. In the next section, the concept of multiscale fundamental forms is introduced. In section 3, a strategy for image fusion is elaborated and experiments on multispectral Landsat images are performed to test the technique and compare it to standard wavelet fusion. In section 4, a strategy for image merging is developed and experiments on SPOT panchromatic and multispectral Landsat images are performed to test and compare the technique to standard wavelet merging.

II. VECTOR-VALUED EDGE REPRESENTATION USING MULTISCALE FUNDAMENTAL FORMS

A. The first fundamental form

For the derivation of the first fundamental form, we will follow [1]. Let $\mathbf{I}(x, y)$ be a vector-valued image with components $I_n(x, y)$, $n = 1, \dots, N$. The value of \mathbf{I} at a given point is a N -dimensional vector. To describe the gradient information of \mathbf{I} , let us look at the differential of \mathbf{I} . In a Euclidean space:

$$d\mathbf{I} = \frac{\partial \mathbf{I}}{\partial x} dx + \frac{\partial \mathbf{I}}{\partial y} dy \quad (1)$$

and its squared norm is given by (sums are over all bands of the image):

$$\begin{aligned} (d\mathbf{I})^2 &= \begin{pmatrix} dx \\ dy \end{pmatrix}^T \begin{pmatrix} \left(\frac{\partial \mathbf{I}}{\partial x}\right)^2 & \frac{\partial \mathbf{I}}{\partial x} \frac{\partial \mathbf{I}}{\partial y} \\ \frac{\partial \mathbf{I}}{\partial x} \frac{\partial \mathbf{I}}{\partial y} & \left(\frac{\partial \mathbf{I}}{\partial y}\right)^2 \end{pmatrix} \begin{pmatrix} dx \\ dy \end{pmatrix} \\ &= \begin{pmatrix} dx \\ dy \end{pmatrix}^T \begin{pmatrix} \sum \left(\frac{\partial I_n}{\partial x}\right)^2 & \sum \frac{\partial I_n}{\partial x} \frac{\partial I_n}{\partial y} \\ \sum \frac{\partial I_n}{\partial x} \frac{\partial I_n}{\partial y} & \sum \left(\frac{\partial I_n}{\partial y}\right)^2 \end{pmatrix} \begin{pmatrix} dx \\ dy \end{pmatrix} \\ &= \begin{pmatrix} dx \\ dy \end{pmatrix}^T \begin{pmatrix} G_{xx} & G_{xy} \\ G_{xy} & G_{yy} \end{pmatrix} \begin{pmatrix} dx \\ dy \end{pmatrix} \end{aligned} \quad (2)$$

This quadratic form is called the first fundamental form (in fact, to be correct, δ_{xy} should be added to G , but this is ignored in most of the literature [2]). It reflects the change in a vector-valued image. The direction of maximal and minimal change are given by the eigenvectors of the 2×2 matrix G . The corresponding eigenvalues denote the rates of change. For a greylevel image ($N = 1$), it is easily calculated that the largest eigenvalue is given by $\lambda_1 = \|\nabla I\|^2$, i.e. the squared gradient magnitude. The corresponding eigenvector lies in the direction of maximal gradient. The other eigenvalue equals zero. For a multivalued image, the eigenvectors and eigenvalues describe an ellipse in the image plane. When $\lambda_1 \gg \lambda_2$, the gradients of all bands are more or less in the same direction. When $\lambda_2 \simeq \lambda_1$, there is no preferential direction. The conjecture is that the multivalued edge information is reflected by the eigenvectors and eigenvalues of the first fundamental form.

A particular problem that occurs is that the diagonalization does not uniquely specify the sign of the eigenvectors. This has been extensively studied in [2]. There, it was proven

that the eigenvectors can be uniquely oriented in simply connected regions where $\lambda_2 \neq \lambda_1$. Based on this, an algorithm was proposed to orient the eigenvectors, keeping the angle continuous in local regions.

B. The dyadic wavelet transform

In this paper, we expand the concept of the first fundamental form towards a multiresolution description. The wavelet transform employed in this work is based on non-orthogonal (redundant) discrete wavelet frames introduced by Mallat [4]. Let $\theta(x, y)$ be a 2-D smoothing function. Supposing θ is differentiable, define

$$\psi^1(x, y) = \frac{\partial\theta(x, y)}{\partial x} \text{ and } \psi^2(x, y) = \frac{\partial\theta(x, y)}{\partial y} \quad (3)$$

The wavelet transform of a greylevel image $I(x, y)$ is then defined by:

$$D_s^1(x, y) = I * \psi_s^1(x, y) \text{ and } D_s^2(x, y) = I * \psi_s^2(x, y) \quad (4)$$

where $*$ denotes the convolution operator and

$$\psi_s^1(x, y) = \frac{1}{s^2} \psi^1\left(\frac{x}{s}, \frac{y}{s}\right) \text{ and } \psi_s^2(x, y) = \frac{1}{s^2} \psi^2\left(\frac{x}{s}, \frac{y}{s}\right) \quad (5)$$

denote the dilations of the functions ψ^i . s is the *scale* parameter which commonly is set equal to 2^j with $j = 1, \dots, d$. This yields the so called *dyadic* wavelet transform of *depth* d . $D_{2^j}^1$ and $D_{2^j}^2$ are referred to as the detail images, since they contain horizontal and vertical details of I at scale j .

In practice, this transform is computed by iterative filtering with a set of low and high pass filters H and G , associated with the wavelets ψ^1 and ψ^2 . These filters have finite impulse responses, which makes the transform fast and easy to implement.

$$\begin{aligned} L_{2^{j+1}}(x, y) &= [H_{j,x} * [H_{j,y} * L_{2^j}]](x, y) \\ D_{2^{j+1}}^1(x, y) &= [d_{j,x} * [G_{j,y} * L_{2^j}]](x, y) \\ D_{2^{j+1}}^2(x, y) &= [G_{j,x} * [d_{j,y} * L_{2^j}]](x, y) \end{aligned} \quad (6)$$

$L_1 = I$ and d is the Dirac filter whose impulse response equals 1 at 0 and 0 otherwise. Thus the wavelet representation of depth d of the image I consists of the *low resolution image* L_{2^d} and *detail images* $\{D_{2^j}^i\}_{j=1, \dots, d}^{i=1, 2}$.

Substitution of (3) and (5) in (4) yields the following interesting property:

$$\begin{pmatrix} D_{2^j}^1(x, y) \\ D_{2^j}^2(x, y) \end{pmatrix} = 2^j \begin{pmatrix} \frac{\partial}{\partial x}(I * \theta_{2^j})(x, y) \\ \frac{\partial}{\partial y}(I * \theta_{2^j})(x, y) \end{pmatrix} = 2^j \nabla(I * \theta_{2^j})(x, y) \quad (7)$$

This stipulates that the wavelet transform of a greylevel image consists of the components of the gradient of the image, smoothed by the dilated smoothing function θ_{2^j} .

C. The multiscale fundamental form

Based on (7), for vector-valued images a fundamental form can be constructed at each scale. Similar to (2), and applying (7), the squared norm of the differential of $(\mathbf{I} * \theta_{2^j})(x, y)$ is given by:

$$\begin{aligned} & (d(\mathbf{I} * \theta_{2^j}))^2 \\ &= 2^{-2j} \begin{pmatrix} dx \\ dy \end{pmatrix}^T \begin{pmatrix} \sum (D_{n,2^j}^1)^2 \sum D_{n,2^j}^1 D_{n,2^j}^2 \\ \sum D_{n,2^j}^1 D_{n,2^j}^2 \sum (D_{n,2^j}^2)^2 \end{pmatrix} \begin{pmatrix} dx \\ dy \end{pmatrix} \\ &= 2^{-2j} \begin{pmatrix} dx \\ dy \end{pmatrix}^T \begin{pmatrix} G_{2^j}^{xx} & G_{2^j}^{xy} \\ G_{2^j}^{xy} & G_{2^j}^{yy} \end{pmatrix} \begin{pmatrix} dx \\ dy \end{pmatrix} \end{aligned} \quad (8)$$

where $D_{n,2^j}^1$ and $D_{n,2^j}^2$ are the j -th scale detail coefficients of the n -th band image. This quadratic form will be referred to as the j -th scale fundamental form. It reflects the change in the j -th scale smoothed image and therefore the edge information at the j -th scale. The direction of maximal and minimal change are given by the eigenvectors $\mathbf{v}_{2^j}^+$ and $\mathbf{v}_{2^j}^-$ of the 2×2 matrices G_{2^j} . The corresponding eigenvalues $\lambda_{2^j}^+$ and $\lambda_{2^j}^-$ denote the rates of change. The eigenvectors and eigenvalues describe an ellipse in the image plane, where the longest axis denotes the direction of the largest gradient at scale j and the shortest axis the variance of gradient at scale j around that direction.

For a greylevel image, one obtains

$$\begin{aligned} \lambda_{2^j}^+(x, y) &= 2^{-2j} [(D_{2^j}^1)^2(x, y) + (D_{2^j}^2)^2(x, y)] = \|\nabla(I * \theta_{2^j})\|^2 \\ \mathbf{v}_{2^j}^+(x, y) &= \frac{\nabla(I * \theta_{2^j})}{\|\nabla(I * \theta_{2^j})\|} \end{aligned} \quad (9)$$

i.e. the first eigenvector denotes the direction of the gradient of the j -th scale smoothed

image, while its corresponding eigenvalue denotes its length. Also remark that:

$$\begin{aligned} D_{2j}^1(x, y) &= \sqrt{\lambda_{2j}^+} v_{2j,x}^+(x, y) \\ D_{2j}^2(x, y) &= \sqrt{\lambda_{2j}^+} v_{2j,y}^+(x, y) \end{aligned} \quad (10)$$

i.e. the original representation of a greylevel image is obtained by projecting the first eigenvector, multiplied by the square root of the corresponding eigenvalue onto the x and y -axes.

In vector-valued images the edge information is contained in both eigenvalues. In this paper, for the purpose of image fusion and merging, the conjecture is made that only the first eigenvector and eigenvalue of the multiscale fundamental forms describe the edge information of a multivalued image in a multiresolution way. The vector-valued image can be represented at each scale by:

$$\begin{aligned} D_{2j}^{1,+}(x, y) &= \sqrt{\lambda_{2j}^+} v_{2j,x}^+(x, y) \\ D_{2j}^{2,+}(x, y) &= \sqrt{\lambda_{2j}^+} v_{2j,y}^+(x, y) \end{aligned} \quad (11)$$

The same problem as in the single scale case occurs: the matrix diagonalization does not uniquely specify the signs of the eigenvectors. This phenomenon translates in the vector-valued image problem as arbitrariness of the gradients orientation. From (11), this orientation reflects on the sign of the detail coefficients that can flip incoherently from one pixel to another. Therefore the orientation must be determined before a reconstruction can be calculated. Instead of following the proposal of [2], we propose a more simple solution to this problem. The orientation of the gradient is approximated by the orientation of the gradient of the average of all bands. The average of the bands is calculated and wavelet transformed. The product of the obtained detail coefficients \overline{D}_{2j}^1 and \overline{D}_{2j}^2 with the first eigenvectors then determines the signs: if $\overline{D}_{2j}^1 v_{2j,x}^+ + \overline{D}_{2j}^2 v_{2j,y}^+ \geq 0$ then the sign of the eigenvector is not changed, if this product is negative, then the sign of $v_{2j,x}^+$ is flipped.

III. MULTISPECTRAL IMAGE FUSION

Image fusion is the process of combining several, perfectly registered images into one greylevel image. This technique is applied on multispectral satellite imagery [20], [21] as well as on biomedical multimodal imagery [22], with the purpose of visualization and

of reducing the complexity for classification and segmentation tasks. Another important application in the literature is the fusion of multisensor imagery as for instance provided by ground based or airborne (military) platforms and surveillance devices [23], [24], [9]. Another important application is found in the automotive industry [18], [25]. In a multiresolution approach, the wavelet representations of all bands are combined into one greylevel image wavelet representation. In [6] the detail coefficients between different bands are compared and for each pixel the largest one is chosen to represent the fused image.

Using the proposed representation, a fusion algorithm can be constructed in the following way. All bands are wavelet transformed using (6). For each scale, the multiscale fundamental forms are calculated using (8). After diagonalization, the wavelet representation (11) is obtained. A low resolution image is obtained by averaging the low resolution images of the original bands: $\bar{L}_{2^d} = \frac{1}{N} \sum_{n=1}^N L_{n,2^d}$. The obtained representation is then given by: \bar{L}_{2^d} and $\{D_{2^j}^{i,+}\}_{j=1,\dots,d}^{i=1,2}$. Reconstruction generates a greylevel image that contains the fused edge information of the different bands. In figure (1) a schematic overview of this fusion algorithm is given.

To demonstrate the proposed fusion technique, the following experiment is conducted. As a test image remote sensing data is used: a Thematic Mapper image from the Huntsville area, Alabama, USA, containing 7 bands of 512x512 images from the U.S. Landsat series of satellites. Two bands (bands 1 and 4) are fused into one greylevel image. In figure (2), the result is shown. Figure (2a) and (2b) show the two original bands. Two dominant features, a river and a builded area are clearly visible in one of the bands, and hardly visible in the other band. In figure (2c), the result of the proposed technique is shown. In figure (2d), the result of the wavelet fusion technique of [6] is shown. The same wavelet redundant wavelet representation as in the first image is applied on every band. For each pixel position and at each scale, the largest absolute detail coefficient of the different bands is taken to be the detail coefficient of the fused image: $\tilde{D}_{2^j}^i(x, y) = \max_n |D_{n,2^j}^i(x, y)|$.

One can observe that both features, the river and the builded area are clearly visible in both fused results. This experiments merely shows that the proposed fusion technique visually leads to similar results as the wavelet-based fusion techniques from the literature. The proposed technique appears to have an improved overall contrast compared to the

wavelet maxima procedure, but it is hard to quantify these results. For this, human observer experiments should be performed. For fusion, particular task performance has been studied [26], [27], [28], [29], [30]. In the next section, we will demonstrate that the proposed technique is extremely useful for a specific fusion process, namely the merging of multispectral images.

IV. MULTISPECTRAL IMAGE MERGING

A problem, related to image fusion is that of image merging. This technique is applied in multispectral satellite imagery, where e.g. a high-resolution greylevel image is merged into a lower resolution multispectral image to enhance its spatial resolution. A typical application is given by merging a high-resolution SPOT Panchromatic image with a lower-resolution Landsat Thematic Mapper multispectral image to improve the spatial resolution of the latter, while preserving its spectral resolution.

We design a merging procedure in the following way. Each band of the multispectral image is merged with the panchromatic image into one representation, using (11). To preserve the spectral information, the low resolution image of the multispectral bands wavelet representation is retained. The merged bands wavelet representation is now given by $L_{n,2^d}, \{D_{2^j}^{i,+}\}_{j=1,\dots,d}^{i=1,2}$. After reconstruction, this leads to an merged result from the original band and the panchromatic image.

To compare, the substitution techniques from the literature are applied. Two different techniques are used. In the first, the detail images of each band of the multispectral image are replaced by the detail images of the panchromatic image [13]. We will refer to this technique as MERGE1. In the second approach, the same replacement takes place, but on top of this, the low-resolution wavelet images of each band of the multispectral image are replaced by the original bands [15]. We will refer to this technique as MERGE2.

The following experiments are conducted. In the first experiment, band 1 of a Landsat Thematic Mapper 7-band image is used to form a (high-resolution) panchromatic image. In the mean time, 3 bands of the image are chosen to form a color image (band 7 is Red, band 4 is Green and band 2 is Blue) , that is smoothed (with a gaussian mask with $\sigma = 5$) to represent a lower-resolution multispectral image. The same image as before is used. In figure 3, the panchromatic and the multispectral image (intensity only) are

shown. Merging is performed using MERGE1, MERGE2 and the proposed technique. The resulting multispectral images (intensity only) are shown in figure 4.

Two main features are visible in the images: a river and a builded area. The images are composed in such a way that one of the features (the river) is visible in the multispectral image, but hardly visible in the panchromatic image, while the other feature (the builded area) is mainly visible in the panchromatic image. By using replacement as a merging rule, the features that are not present in the panchromatic image will be discarded. The proposed merging rule however will still take the lower-resolution edge information from the multispectral image into account. The difference can be clearly observed in the merged images. The proposed technique displays the river with much higher resolution than the two other techniques, while the overall contrast and resolution of the remaining of the images is comparable.

In the second experiment, A SPOT Panchromatic image is merged with a three-band Landsat multispectral image. The SPOT image has a resolution of $10m$, while the Landsat images have a resolution of $30m$. Again, the merging procedure aims at enhancing the spatial resolution of the multispectral image by merging it with the high-resolution spatial information of the panchromatic image. In this experiment, the differences in spatial resolution are smaller than in the previous experiment. Therefore, the differences in spatial resolution between the different merged results will be visually smaller. However, the preservation of the spectral resolution is also an important issue. The aim of this experiment is to demonstrate that the proposed technique better preserves the spectral information. To compare we will adopt the two wavelet-based mergers MERGE1 and MERGE2, and a standard merging method, based on the Intensity-Hue-Saturation transformation [31]. Here, the multispectral image is IHS-transformed, and the panchromatic image is merged into the I-component. We will refer to this technique as IHS.

In figure 5, the original SPOT and Landsat images are displayed. In figure 6, the merged results are shown, using IHS and MERGE1 (intensity only). In figure 7a and c, the merged result using the proposed technique and MERGE2 (color versions) is shown. With respect to the spectral resolution the results are visually convincing. The spectral information of the proposed technique very much resembles that of the original Landsat image, while

MERGE2 display a poor spectral resolution. The color versions of the merged results of IHS and MERGE1 are not shown here but are similar to the result of MERGE2.

With respect to the spatial resolution, results are visually not really different. In fact, an apparent loss in spatial resolution can be observed using the proposed technique. This effect originates from a saturation of the bright areas in the image. This can be seen by looking at the histograms of the detail images. For the merged result, these are somewhat broader than the histograms of the corresponding original detail images. In order to compensate for this, the histograms are linearly stretched to obtain the same standard deviation as the original. In figure 7b, the result is shown. The apparent loss in spatial resolution has disappeared, while still keeping a superior spectral resolution.

In order to quantify that the spectral information is better preserved using the proposed technique, a pixel-by-pixel comparison of the results with the original spectra is performed. For this, their correlation is calculated. Although it is not really clear whether this metric has any relation with visual perception, it is used regularly. Recently, there have been some attempts to include perception-based metrics [7], [32], [33].

The correlation between 2 images A and B is defined as:

$$Cor(A, B) = \frac{\langle (A - \langle A \rangle)(B - \langle B \rangle) \rangle}{\sqrt{\langle (A - \langle A \rangle)^2 \rangle \langle (B - \langle B \rangle)^2 \rangle}} \quad (12)$$

where $\langle . \rangle$ denotes the average over all pixels. This number is calculated for the R, G and B bands separately. In table 1, results are shown. It is clear that all wavelet-based techniques better preserve spectral information than the IHS technique. The obtained values from the IHS technique and the wavelet techniques from the literature agree with perviously reported results [13]. The proposed technique outperforms the other two wavelet mergers.

Spectral preservation is an important issue, not only for visual purposes, but also for specific task performance. Many applications perform classification based on the spectral information. It is clear from the images and from the correlation measure that the proposed technique will outperform the others with respect to classification. To show this, we measured the average spectral response of a small homogeneous green area in the original Landsat image (pointed to by an arrow in figure 5b, and the same area in the merged images. The (Euclidean) distance in the RGB-space between the cluster centers of the

original and the merged results where 269, 180, 169 and 74 for IHS, MERGE1, MERGE2 and the proposed technique. Similar experiment were performed at other regions, leading to similar results.

Finally, the following classification experiment is performed. The original Landsat image is segmented by clustering its RGB-space. For this, we applied the k-means clustering algorithm, with $k = 4$. The pixels, belonging to one of the clusters are shown in figure 8a, revealing the objects that have a spectral response, corresponding to that specific cluster. In figure 8b and c, we measure the same spectral response (i.e. display all the pixels that belong to the same cluster), on the merged images, using MERGE2 and the proposed technique respectively. One can notice that most of the objects have disappeared when using MERGE2, while most of the objects have been classified using the proposed technique, due to its ability to preserve spectral resolution. Moreover, the objects clearly have improved in spatial resolution.

V. CONCLUSIONS

We have proposed a new wavelet representation for multispectral images. The representation is based on the concept of multiscale fundamental forms, a multiresolution extension of the first fundamental form, that describes edge information of multivalued images. Based on the representation, multispectral image fusion and image merging techniques are proposed. Experiments are conducted for fusion and merging of multispectral satellite images. Landsat TM images are fused and merged with SPOT panchromatic images. The proposed techniques are demonstrated to outperform other wavelet-based merging techniques.

REFERENCES

- [1] S. Di Zenzo, “A note on the gradient of a multi-image,” *Comput. Vision Graphics Image Processing*, vol. 33, pp. 116–125, 1986.
- [2] A. Cumani, “Edge detection in multispectral images,” *CVGIP: Graphical Models and Image Processing*, vol. 53, pp. 40–51, 1991.
- [3] G. Sapiro and D.L. Ringach, “Anisotropic diffusion of multivalued images with applications to color filtering,” *IEEE Trans. Image Processing*, vol. 5, 11, pp. 1582–1586, 1996.
- [4] S. Mallat and S. Zhong, “Characterization of signals from multiscale edges,” *IEEE Trans. Pattern Anal. Machine Intell.*, vol. 14, pp. 710–732, 1992.
- [5] C. Pohl and J. Van Genderen, “Multisensor image fusion in remote sensing: concepts, methods and applications,” *Int. J. Remote Sensing*, vol. 19, pp. 823–854, 1998.
- [6] H. Li, B.S. Manjunath, and S.K. Mitra, “Multisensor image fusion using the wavelet transform,” *Graphical Models and Image Processing*, vol. 57, no. 3, pp. 235–245, 1995.
- [7] T. Wilson, S. Rogers, and L. Meyers, “Perceptual-based hyperspectral image fusion using multiresolution analysis,” *Optical Engineering*, vol. 34 (11), pp. 3154–3164, 1995.
- [8] T. Wilson, S. Rogers, and L. Meyers, “Perceptual-based image fusion for hyperspectral data,” *IEEE T. Geosci. Rem. Sensing*, vol. 35 (4), pp. 1007–1017, 1997.
- [9] T. Pu and G. Ni, “Contrast-based image fusion using the discrete wavelet transform,” *Optical Engineering*, vol. 39 (8), pp. 2075–2082, 2000.
- [10] D.A. Yocky, “Image merging and data fusion by means of the discrete two-dimensional wavelet transform,” *J. Opt. Soc. Am. A*, vol. 12, no. 9, pp. 1834–1841, 1995.
- [11] B. GarguetDuport, “The use of multiresolution analysis and wavelets transform for merging spot panchromatic and multispectral image data,” *Photogramm. Eng. Rem. S.*, vol. 62 (9), pp. 1057–1066, 1996.
- [12] B. GarguetDuport, “Wavemerg: A multiresolution software for merging spot panchromatic and spot multispectral data,” *Environmental Modelling and Software*, vol. 12 (1), pp. 85–92, 1997.
- [13] D.A. Yocky, “Multiresolution wavelet decomposition image merger of landsat the-

- matic mapper and spot panchromatic data,” *Photogramm. Engin. and Remote Sensing*, vol. 62, pp. 1067–1074, 1996.
- [14] J. Zhou, D. Civco, and J. Silander, “A wavelet transform method to merge landsat tm and spot panchromatic data,” *Intern. J. Rem. Sensing*, vol. 19 (4), pp. 743–757, 1998.
- [15] J. Nunez, X. Otazu, O. Fors, A. Prades, V. Pala, and R. Arbiol, “Image fusion with additive multiresolution wavelet decomposition; applications to spot+landsat images,” *J. Opt. Soc. Am. A*, vol. 16, pp. 467–474, 1999.
- [16] J. Nunez, X. Otazu, O. Fors, A. Prades, V. Pala, and R. Arbiol, “Multiresolution-based image fusion with additive wavelet decomposition,” *IEEE T. Geosci. Rem. Sensing*, vol. 37 (3), pp. 1204–1211, 1999.
- [17] T. Ranchin and L. Wald, “Fusion of high spatial and spectral resolution images: the arsis concept and its implementation,” *Photogramm. Engin. and Remote Sensing*, vol. 66, pp. 49–61, 2000.
- [18] F. Jahard, D.A. Fish, A.A. Rio, and C.P. Thompson, “Far/near infrared adapted pyramid-based fusion for automotive night vision,” in *Sixth International Conference on Image Processing and its Applications*, 1997, pp. 886–890.
- [19] B. Ajazzi, L. Alparone, S. Baronti, and R. Carla, “Assessment of pyramid-based multisensor image data fusion,” in *Image and Signal Processing for Remote Sensing*, S.B. Serpico, Ed., 1998, vol. IV, pp. 237–248.
- [20] I.L. Thomas, V.M. Benning, and N.P. Ching, *Classification of remotely sensed images*, Adam Hilger, Bristol, 1987.
- [21] C Lee and D.A. Landgrebe, “Analyzing high-dimensional multispectral data,” *IEEE Trans. Geosci. Remote Sensing*, vol. 31, no. 4, pp. 388–400, 1993.
- [22] T. Taxt and A. Lundervold, “Multispectral analysis of the brain using magnetic resonance imaging,” *IEEE Trans. Med. Imaging*, vol. 13, no. 3, pp. 470–481, 1994.
- [23] Y. Carts-Powell, “Fusion ccd and ir images creates color night vision,” *Laser Focus World*, vol. 32(5), pp. 32–36, 1996.
- [24] N. Nandhakumar and J.K. Aggarwal, “Integrated analysis of thermal and visual images for scene interpretation,” *IEEE Transactions on Pattern Analysis and Machine*

- Intelligence*, vol. 10(4), pp. 469–481, 1988.
- [25] W.K. Krebs, J.S. McCarley, T. Kozek, G.M. Miller, M.J. Sinai, and F.S. Werblin, “An evaluation of a sensor fusion system to improve drivers’ nighttime detection of road hazards,” in *Annual Meeting Human Factors and Ergonomics Society*, 1999, pp. 1333–1337.
- [26] D. Ryan and R. Tinkler, “Night pilotage assessment of image fusion,” in *SPIE Proceedings on Helmet and Head Mounted Displays and Symbology Design Requirements II*, R.J. Lewadowsky, W. Stephens, and L.A. Haworth, Eds., 1995, pp. 50–67.
- [27] P.M. Steele and P. Perconti, “Part task investigation of multispectral image fusion using gray scale and synthetic color night vision sensor imagery for helicopter pilotage,” in *Proceedings of the SPIE Conference on Targets and Backgrounds, Characterization and Representation III*, W. Watkins and D. Clement, Eds., 1997, pp. 88–100.
- [28] E.A. Essock, M.J. Sinai, J.S. McCarley, W.K. Krebs, and J.K. Deford, “Perceptual ability with real-world nighttime scenes: image-intensified, infrared and fused-color imagery,” *Human Factors*, vol. 41(3), pp. 438–452, 1999.
- [29] M. Aguilar, D.A. Fay, D.B. Ireland, J.P. Racamoto, W.D. Ross, and A.M. Waxman, “Field evaluations of dual-band fusion for color night vision,” in *SPIE Conference on Enhanced and Synthetic Vision 1999*, J.G. Verly, Ed., 1999, pp. 168–175.
- [30] J. Sinai, J.S. McCarley, and W.K. Krebs, “Scene recognition with infra-red, low-light and sensor fused imagery,” in *Proceedings of the IRIS Specialty Groups on Passive Sensors*, 1999, pp. 1–9.
- [31] W.J. Carper, T.M. Lillesand, and R.W. Kiefer, “The use of intensity-hue-saturation transformations for merging spot panchromatic and multispectral image data,” *Photogram. Eng. Remote Sens.*, vol. 56, pp. 459–467, 1990.
- [32] M.E. Ulug and L. Claire, “A quantitative metric for comparison of night vision fusion algorithms,” in *Sensor Fusion: Architectures, Algorithms and Applications IV*, B.V. Dasarathy, Ed., 2000, pp. 80–88.
- [33] C.S. Xydeas and V.S. Petrovic, “Objective pixel-level image fusion performance measure,” in *Sensor Fusion: Architectures, Algorithms and Applications IV*, B.V. Dasarathy, Ed., 2000, pp. 89–98.

FIGURE CAPTIONS

Fig. 1:

Schematic overview of the multiscale fusion algorithm.

Fig. 2:

Fusion of 2 bands of a Landsat image; a: original band 1; b: original band 4; c: fused result using the proposed technique; d: fused result using wavelet maxima fusion.

Fig. 3:

a: Original high-resolution panchromatic and b: low-resolution multispectral images.

Fig. 4:

Results of merging the images of figure 3, using a: MERGE1, b: MERGE2 and c: the proposed technique.

Fig. 5:

a: Original SPOT and b: Landsat images.

Fig. 6:

Merged images from figure 5, using a: IHS, b: MERGE1.

Fig. 7:

Merged images from figure 5, using the proposed technique; a: before and b: after histogram adaption; c: using MERGE2.

Table 1:

Correlations for the merged results using IHS, MERGE1, MERGE2 and the proposed technique, without and with histogram adaption.

Fig. 8:

Spectral response after k-means clustering a: on the original Landsat image; b: on the

merged image, using MERGE2; c: on the merged image, using the proposed technique.

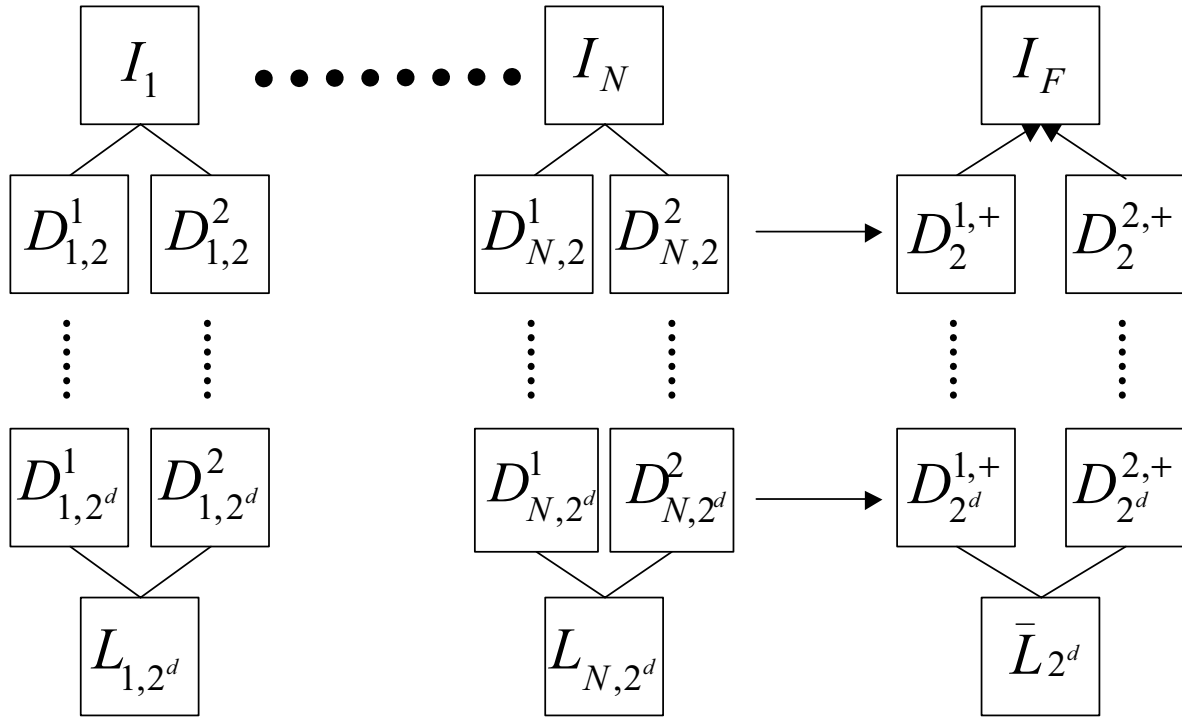


Fig. 1. Schematic overview of the multiscale fusion algorithm

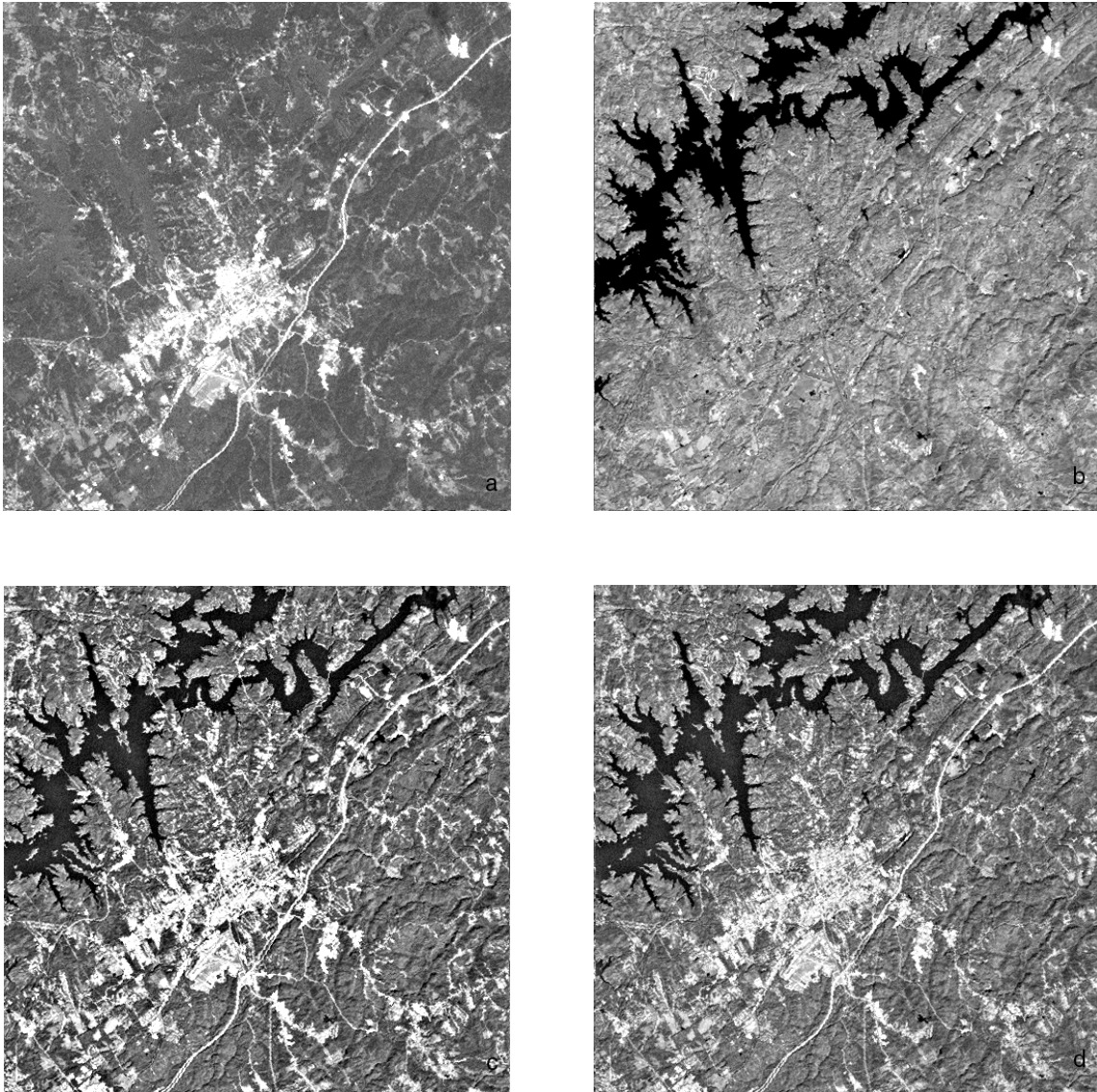


Fig. 2. Fusion of 2 bands of a Landsat image; a: original band 1; b: original band 4; c: fused result using the proposed technique; d: fused result using wavelet maxima fusion

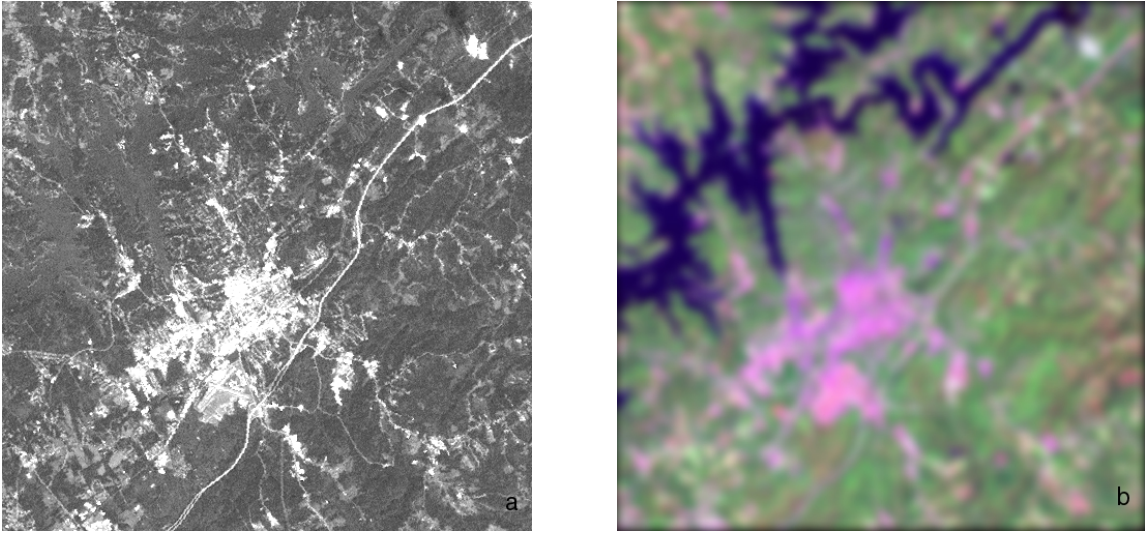


Fig. 3. a: Original high-resolution panchromatic and b: low-resolution multispectral images



Fig. 4. Results of merging the images of figure 3, using a: MERGE1, b: MERGE2 and c: the proposed technique

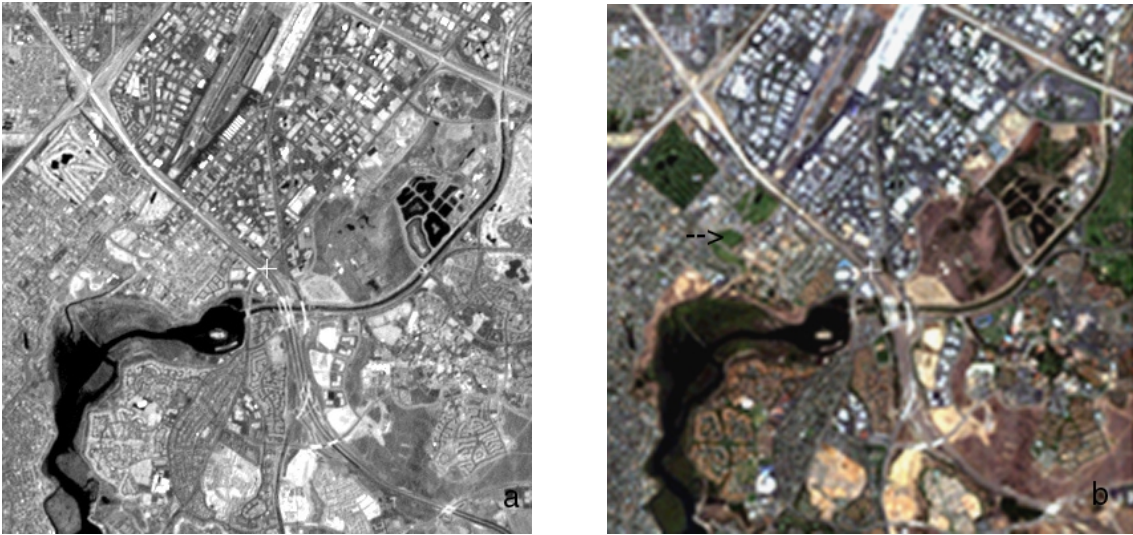


Fig. 5. a: Original SPOT and b: Landsat images



Fig. 6. Merged images from figure 5, using a: IHS, b: MERGE1

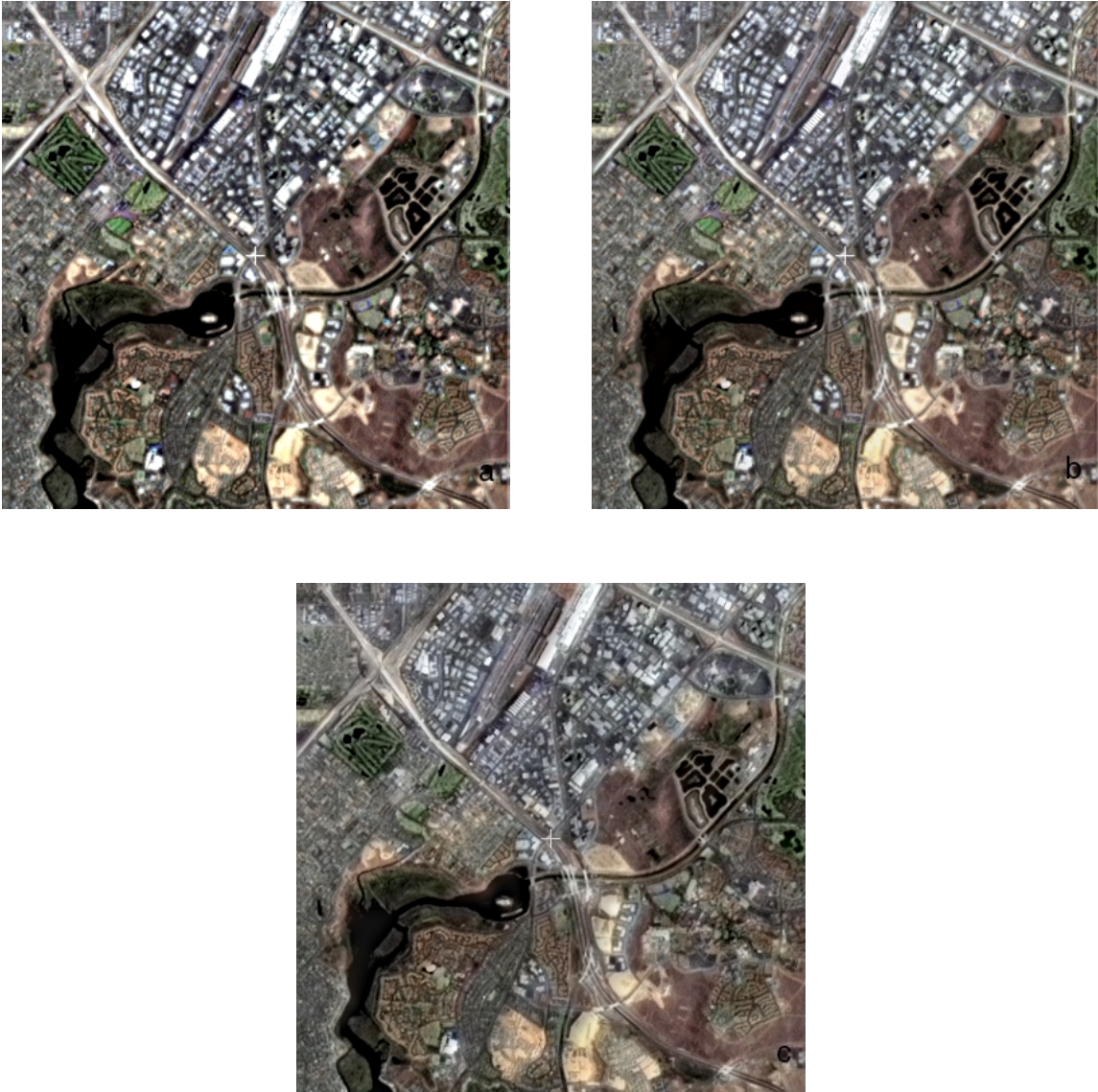


Fig. 7. Merged images from figure 5, using the proposed technique, a: before and b: after histogram adaption; c: using MERGE2

TABLE I

CORRELATIONS FOR THE MERGED RESULTS USING IHS, MERGE1, MERGE2 AND THE PROPOSED
TECHNIQUE, BEFORE AND AFTER HISTOGRAM ADAPTION

	IHS	MERGE1	MERGE2	Proposed, before	after histogram adaption
R	0.69	0.81	0.78	0.92	0.92
G	0.69	0.83	0.80	0.92	0.93
B	0.66	0.78	0.76	0.90	0.91

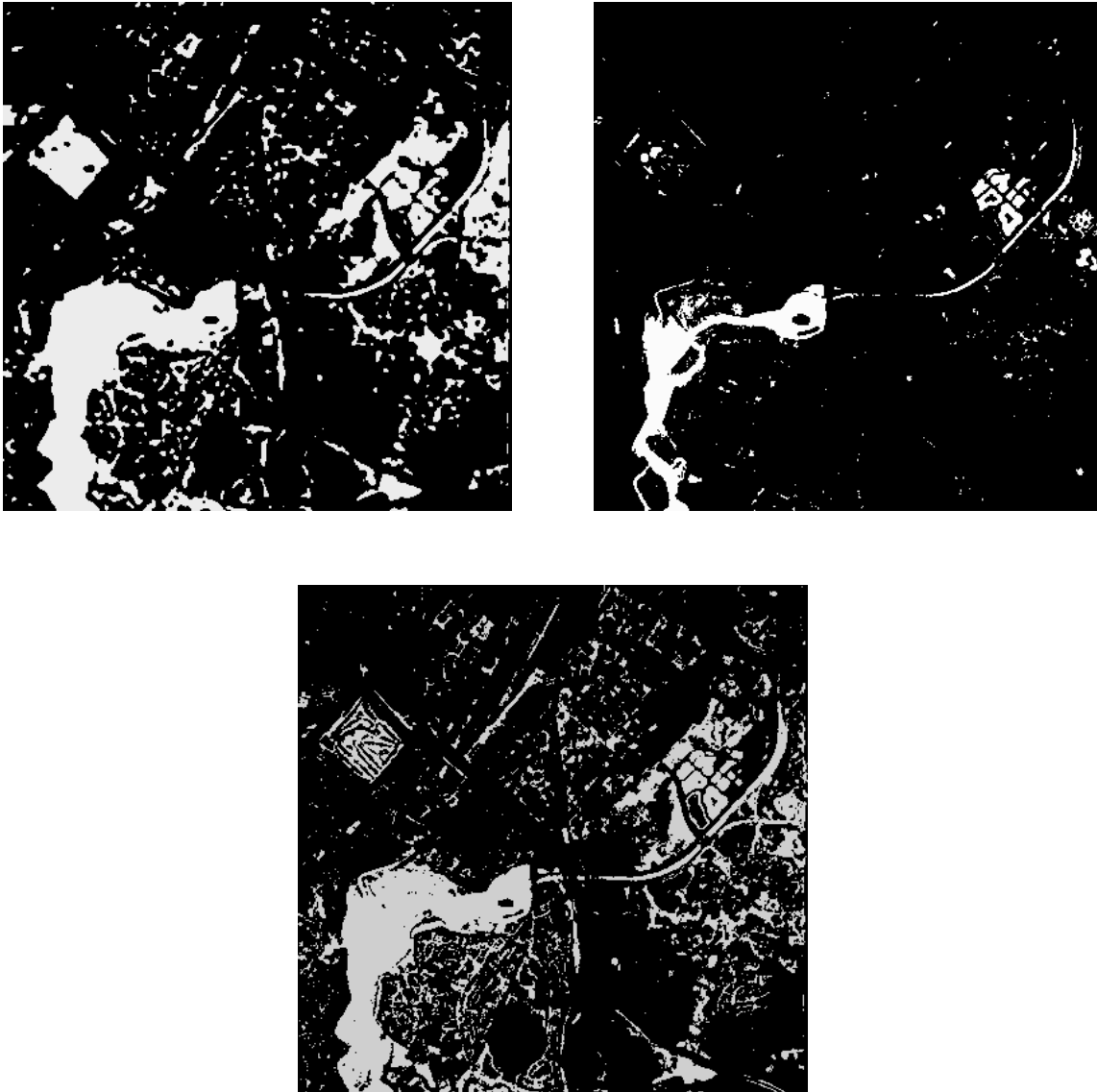


Fig. 8. Spectral response after k-means clustering a: on the original Landsat image; b: on the merged image, using MERGE2; c: on the merged image, using the proposed technique.